Nuclear Science and Techniques (2025) 36:202
https://doi.org/10.1007/s41365-025-01786-1

The impact of tensor force on collective correlations and neutrinoless double-β decay

Chang-Feng Jiao[1,2] · **Cen-Xi Yuan**[3]

Received: 22 March 2025 / Revised: 27 May 2025 / Accepted: 5 June 2025 / Published online: 14 August 2025

Abstract

The tensor force changes the nuclear shell structure and thus may result in underlying influence of the collectivity and decay properties of the nucleus. We carefully examined the impact of the monopole and multipole effects originating from the tensor force on both the collectivity and the matrix element for the neutrinoless double-β ($0\nu\beta\beta$) decay, using the generator-coordinate method with an effective interaction. To analyze the effect of the tensor force, we employed an effective Hamiltonian associated with the monopole-based universal interaction that explicitly consists of the central, tensor, and spin–orbit coupling terms. The interferences among the shell structure, quadrupole collectivity, nucleon occupancy, and $0\nu\beta\beta$ matrix elements were analyzed in detail. A better understanding of the tensor force would be of great importance in reducing the theoretical uncertainty in $0\nu\beta\beta$ nuclear matrix element calculations.

Keywords Neutrinoless double-beta decay · Collective correlations · Tensor force

1 Introduction

The prospect of observing neutrinoless double-β ($0\nu\beta\beta$) decay is of great interest, as it would be the most feasible way to verify the Majorana nature of neutrinos, and thus demonstrate lepton-number violation [1–5]. In addition, the measurement of its half-life can provide access to the scale for the absolute neutrino mass and mass hierarchy, but it requires a reliable description of the underlying nuclear matrix elements (NMEs) governing the $0\nu\beta\beta$ decay [6, 7]. More practically, accurate values of NME are crucial for concluding a definitive choice and the amount of material required in complicated and expensive $\beta\beta$-decay experiments. Because $0\nu\beta\beta$ decay involves unknown neutrino properties, such as the neutrino mass scale, the matrix element cannot be measured. On the other hand, it strongly depends on the underlying nuclear structures of the parent and daughter nuclei; hence, it must be calculated using nuclear structure methods. At present, NMEs obtained by various theoretical approaches differ by a factor of up to three [7, 8]. Therefore, reducing the uncertainty in matrix elements is a crucial goal for the nuclear structure community.

An important factor in diminishing the uncertainty is a better description of the ground-state (g.s.) wave functions for both parent and daughter nuclei. To achieve this goal, there are two main issues that need to be addressed: understanding the many-body correlations and the nucleon–nucleon interactions that are strongly relevant to the $0\nu\beta\beta$ decay NMEs. For the former issue, it was found that some collective correlations significantly influence the calculations of $0\nu\beta\beta$ decay matrix elements. In particular, matrix elements were suppressed when the ground states

This work was supported by the National Natural Science Foundation of China (No.12275369), the Fundamental Research Funds for the Central Universities, Sun Yat-sen University (No. 22qntd3101), and the Guangdong Major Project of Basic and Applied Basic Research (2021B0301030006).

✉ Chang-Feng Jiao
jiaochf@mail.sysu.edu.cn

✉ Cen-Xi Yuan
yuancx@mail.sysu.edu.cn

[1] School of Physics and Astronomy, Sun Yat-sen University, 519082 Zhuhai, China

[2] Guangdong Provincial Key Laboratory of Quantum Metrology and Sensing, Sun Yat-sen University, 519082 Zhuhai, China

[3] Sino-French Institute of Nuclear Engineering and Technology, Sun Yat-sen University, 519082 Zhuhai, China

of the parent and daughter nuclei exhibited different intrinsic deformations. This suppression was originally investigated using axial quadrupole collectivity [9–12], and later extended to non-axial quadrupole [13] and octupole correlations [14]. It has also been noticed that the transition operators of $\beta\beta$ decay are sensitive to pairing correlations [11, 12, 15, 16]. The $0\nu\beta\beta$ decay would be favored if one considers like-particle pairing fluctuations [17], but is remarkably hindered by taking into account of proton–neutron (pn) pairing [18–21]. Thus, fully capturing the interplay among collective degrees of freedom is of particular importance for improving the accuracy of the $0\nu\beta\beta$ decay NMEs.

To unveil the interplay between collectivity and $0\nu\beta\beta$ NMEs, we need a nuclear structure method that can be applied to the investigation of $0\nu\beta\beta$ decay and is capable of dealing with multiple collective correlations in an explicit way. The nuclear structure methods that are most commonly used in the $0\nu\beta\beta$ decay matrix-element calculations are the interacting shell model (ISM) [22–30], interacting boson model (IBM) [31–33], quasiparticle random phase approximation (QRPA) [18, 19, 34–43], and generator-coordinate method (GCM) [10–14, 17, 20, 44, 45]. Among them, the so-called quantum number-projected GCM (PGCM) [13, 44, 45] is appealing because it can treat fluctuations in multiple collective correlations explicitly on the same footing, providing a feasible way to evaluate the interference among different correlations. It has been shown that the inclusion of quadrupole and pn-pairing correlations in GCM calculations [13, 21, 44] significantly diminishes the large deviation in the $0\nu\beta\beta$ decay NMEs between the previous GCM and SM predictions. This indicates that the GCM approach captures most of the correlations around the Fermi surface, which are important for $0\nu\beta\beta$ decay.

The other key point is to improve the nucleon–nucleon interaction. To evaluate whether an effective interaction is reasonable for $0\nu\beta\beta$ NME calculations, it would be of particular interest to study the influence of a specific term on the interaction. It has been shown that the tensor force has a unique and robust effect on the single-particle energies of nuclei throughout the nuclear chart, and hence, changes the occupation of nucleons associated with the shell structure [46, 47]. Consequently, the tensor force interferes with the collective motion of the nucleons. For example, occupying specific orbits would provide a larger deformation-driving effect, inducing enhanced quadrupole collectivity. Changing the level density of single-particle orbits around the Fermi surface strongly affects the pairing correlations. Recently, the tensor force has been found to contribute significantly to the low-lying Gamow–Teller distribution and hence makes a dramatic improvement in predicting single-β decay half-lives [48]. Therefore, it is very intriguing to evaluate the impact of the tensor force on collective correlations and the resulting effect on $0\nu\beta\beta$ decay.

To demonstrate the influence of tensor force, the tensor term should be incorporated into the effective interaction in an explicit and separable form. We propose an analysis of the influence of the tensor force on both the collectivity and the $0\nu\beta\beta$ decay NME for candidate nuclei ^{124}Sn/Te,^{130}Te/Xe, and ^{136}Xe/Ba [5, 49, 50], by applying a PGCM calculation in conjunction with the effective Hamiltonian arising from the monopole-based universal interaction $V_{\rm MU}$ [47] plus a spin–orbit force taken from the M3Y interaction [51]. The $V_{\rm MU}$ interaction consists of the central part given by a Gaussian function in addition to the π- and ρ-meson exchange tensor force, which has been very successful in studying tensor monopole effects in previous works [47]. To quantify the impact of the monopole effect associated with the tensor force, we can either include or exclude the tensor-force term in the effective Hamiltonian. This is similar to a previous study that evaluated the impact of the tensor force on single-β decay [48] by including the tensor force in Skyrme density functionals and the residual interaction in the RPA. Here, we consider only the standard light left-handed Majorana neutrino exchange mass mechanism, as it is the simplest and most studied mechanism of the $0\nu\beta\beta$ decay process.

2 The model

Owing to the shell closure approximation, the $0\nu\beta\beta$ decay NME can be computed in terms of the matrix element of a two-body transition operator between the g.s. wave functions of the parent and daughter nuclei. Our wave functions were modified at short distances using a Jastrow-type short-range correlation (SRC) function in the parameterization of CD-Bonn [38]. A more detailed expression of the matrix element can be found in Ref. [18]. These many-body wave functions, which play a crucial role in the NME calculation, are provided by the GCM. We employed a shell-model effective Hamiltonian ($H_{\rm eff}$) in a valence space whose size is free to choose. In an isospin scheme, $H_{\rm eff}$ can be written as the sum of one- and two-body operators:

$$H_{\rm eff} = \sum_a \epsilon_a \hat{n}_a + \sum_{a\leqslant b,c\leqslant d} \sum_{JT} V_{JT}(ab;cd)\hat{T}_{JT}(ab;cd), \tag{1}$$

where ϵ_a stands for single-particle energies, $V_{JT}(ab;cd)$ stands for two-body matrix elements (TBMEs), $\hat{n}_a$ is the number operator for the spherical orbit a with quantum numbers (n_a, l_a, j_a) and

$$\hat{T}_{JT}(ab;cd) = \sum_{MT_z} A^{\dagger}_{JMTT_z}(ab) A_{JMTT_z}(cd) \tag{2}$$

is the scalar two-body density operator for nucleon pairs in orbits a, b and c, d coupled to quantum numbers J, M, T, and T_z.

With the effective Hamiltonian, the first step is to generate a set of reference states $|\Phi(q)\rangle$ that are quasiparticle vacua constrained to specified expectation values $q_i = \langle \mathcal{O}_i \rangle$ for different collective operators $\mathcal{O}_i$. Large-amplitude fluctuations in multiple collective correlations should be treated by further admixing these reference states. Here we take the operators $\mathcal{O}_i$ which encompass the collective coordinates most important for low-lying spectra, and the $0\nu\beta\beta$ NMEs [21]:

$$\begin{aligned} \mathcal{O}_1 &= Q_{20}, & \mathcal{O}_2 &= Q_{22}, \\ \mathcal{O}_3 &= \frac{1}{2}(P_0 + P_0^\dagger), & \mathcal{O}_4 &= \frac{1}{2}(S_0 + S_0^\dagger), \end{aligned} \tag{3}$$

where the operator $P_0^\dagger$ ($S_0^\dagger$) creates a correlated isoscalar (isovector) proton–neutron pair in a single-particle orbit. A detailed definition of collective operators can be found in Ref. [13]. We do not incorporate the fluctuations in like-particle pairing which, according to the EDF-based work of Ref. [17], slightly increases the NMEs. We can treat these fluctuations on an equal footing as those in deformation and pn pairing, but at the cost of a tremendous increase in computing time.

We further solved the constrained Hartree–Fock–Bogoliubov (HFB) equations for the Hamiltonian with linear constraints:

$$\begin{aligned} \langle H' \rangle = \langle H_{\rm eff} \rangle &- \lambda_Z(\langle N_Z \rangle - Z) - \lambda_N(\langle N_N \rangle - N) \\ &- \sum_i \lambda_i(\langle \mathcal{O}_i \rangle - q_i), \end{aligned} \tag{4}$$

where the N_Z and N_N are the proton and neutron number operators, respectively, λ_Z and λ_N are the corresponding Lagrange multipliers. The sum over i includes the quadrupole operators Q_{20} and Q_{22}, with the addition of the isoscalar or isovector proton–neutron pairing operator in Eq. (3). The λ_i represents the Lagrange multipliers that constrain the expected values of these operators to the specified quantities of q_i. We solved these equations many times, constraining each time to a different point on a mesh in the space of q_i.

Once we obtain a set of HFB vacua constrained to various collective correlations, the GCM state can be composed of a linear superposition of the projected HFB vacua, given by

$$|\Psi^J_{NZ\sigma}\rangle = \sum_{K,q} f^{JK}_{q\sigma} |JMK;NZ;q\rangle, \tag{5}$$

where $|JMK;NZ;q\rangle \equiv \hat{P}^J_{MK}\hat{P}^N\hat{P}^Z|\Phi(q)\rangle$. Here, $\hat{P}'$s project HFB states onto a well-defined angular momentum J and its z-component M, neutron number N, and proton number Z [52]. The weight function $f^{JK}_{q\sigma}$, where σ is simply an enumeration index, can be obtained by solving the Hill–Wheeler equations [52]:

$$\sum_{K',q'} \left\{ \mathcal{H}^J_{KK'}(q;q') - E^J_\sigma \mathcal{N}^J_{KK'}(q;q') \right\} f^{JK'}_{q'\sigma} = 0, \tag{6}$$

where the Hamiltonian kernel $\mathcal{H}^J_{KK'}(q;q')$ and the norm kernel $\mathcal{N}^J_{KK'}(q;q')$ are given by:

$$\begin{aligned} \mathcal{H}^J_{KK'}(q;q') &= \langle \Phi(q)|H_{\rm eff}\hat{P}^J_{KK'}\hat{P}^N\hat{P}^Z|\Phi(q')\rangle, \\ \mathcal{N}^J_{KK'}(q;q') &= \langle \Phi(q)|\hat{P}^J_{KK'}\hat{P}^N\hat{P}^Z|\Phi(q')\rangle. \end{aligned} \tag{7}$$

To solve Eq.(6), we diagonalize the norm kernel $\mathcal{N}$ and use the nonzero eigenvalues and the corresponding eigenvectors to construct a set of "natural states". The Hamiltonian is then diagonalized in the space of these natural states to obtain the GCM states $|\Psi^J_{NZ\sigma}\rangle$ (see details in Refs. [53, 54]). With the lowest $J = 0$ GCM states as the ground states of the initial and final nuclei, we can calculate the $0\nu\beta\beta$ decay matrix element $M^{0\nu}$.

3 Effective hamiltonian

The nuclear interaction V can be divided into the central part ($V_{\rm C}$), spin–orbit part ($V_{\rm LS}$), and tensor part ($V_{\rm T}$), as follows :

$$V = V_{\rm C} + V_{\rm LS} + V_{\rm T}. \tag{8}$$

The so-called *jj*55-shell configuration space that comprises the proton and neutron $0g_{7/2}$, $1d_{5/2}$, $1d_{3/2}$, $2s_{1/2}$, and $0h_{11/2}$ orbitals is used for the calculations of ^{124}Sn−Te, ^{130}Te−Xe, and ^{136}Xe−Ba.

The monopole-based universal interaction, $V_{\rm MU}$ [47], and the M3Y type spin–orbit interaction [51] ($V_{\rm MU}$+LS) are used to construct the effective Hamiltonian in the present work. $V_{\rm MU}$ contains a central force in the Gaussian form ($V_{\rm C}$) and a bare $\pi + \rho$ meson exchange tensor force ($V_{\rm T}$). ISM investigations, with $V_{\rm MU}$+LS mainly as the cross–shell interaction, have been performed in various regions and generally agreed with experimental data [55], such as in *psd* [56], *sdpf* [57], *pfsdg* regions [58], ^{132}Sn [59], and ^{208}Pb [60–62] regions. Recently, $V_{\rm MU}$+LS was used, as a unified interaction, to study the excitation energies of medium-heavy nuclei around ^{132}Sn and ^{208}Pb [63, 64]. Compared to $V_{\rm MU}$ proposed in Ref. [47], the proton–proton (neutron–neutron) central forces in the present work were enhanced by 15% (5%), following the suggestions in Refs. [63, 64] to further improve the calculation accuracy of the low-lying excitation energies of medium-heavy nuclei. The constructed Hamiltonian is examined in Sect. 4 along with the discussion of the corresponding results.

4 Results and discussion

An important probe for deformation and associated collectivity is the γ-ray spectroscopy of the nucleus. Figure 1 shows the low-lying level spectra of ^{124}Sn, ^{124}Te, ^{130}Te, ^{130}Xe, ^{136}Xe, and ^{136}Ba obtained with or without the tensor term compared to the experimental data [55]. Although our calculated 6^+ states are overestimated, most of the low-lying states obtained by our calculations, which include the tensor term, are in reasonable agreement with the experimental spectra. The overestimation of higher spin states could be due to the fact that the GCM calculations exclude vibrational motion and broken-pair excitation, while these two excitation modes may significantly lower the excited states, especially in the nearly spherical and weakly deformed nuclei. In general, the inclusion of the tensor term significantly improved the calculated spectra. The 2_1^+ and 4_1^+ states are lowered if the tensor term is included, implying an increase in the quadrupole collectivity owing to the impact off the tensor force.

The reduced $E2$ transition probability, $B(E2:0_1^+\rightarrow 2_1^+)$, provides another direct probe for quadrupole collectivity. It should be noted that there was an inconsistency in the calculations for $B(E2:0_1^+\rightarrow 2_1^+)$ in this region. Using the same SVD interaction, an effective charge set of $e_{\rm n}^{\rm eff}=0.88e$ and $e_{\rm p}^{\rm eff}=1.88e$ was suggested for ^{124}Sn/Te in Refs. [28], but a set of $e_{\rm n}^{\rm eff}=0.5e$ and $e_{\rm p}^{\rm eff}=1.5e$ was used for ^{130}Te/Xe and ^{136}Xe/Ba [27]. This inconsistency was resolved using our effective interaction. In the current work, we used the canonical effective charges $e_{\rm n}^{\rm eff}=0.5e$ and $e_{\rm p}^{\rm eff}=1.5e$ for all the investigated nuclei. The results are compared in Fig. 2 with the experimentally adopted values [65]. A strong agreement is obtained between the calculated and adopted values of $B(E2:0_1^+\rightarrow 2_1^+)$ with the universal effective charges, indicating an improved description of the quadrupole collectivity in these candidate nuclei. This improvement is crucial for reducing uncertainty in the calculation of the $0\nu\beta\beta$ decay matrix.

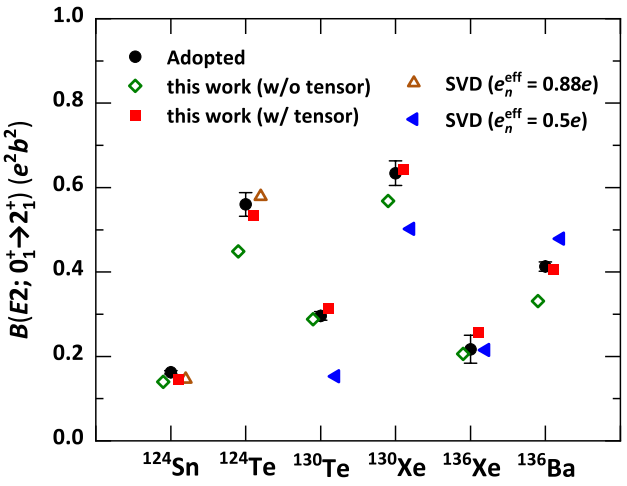

Fig. 2 (Color online) Calculated $B(E2:0_1^+\rightarrow 2_1^+)$ (in e^2b^2) obtained by using the PGCM with the *jj*55 Hamiltonian excluding or including the tensor term, compared to the adopted values [65]

Similar to low-lying γ-ray spectroscopy, incorporating the tensor force results in the enhancement of the quadrupole

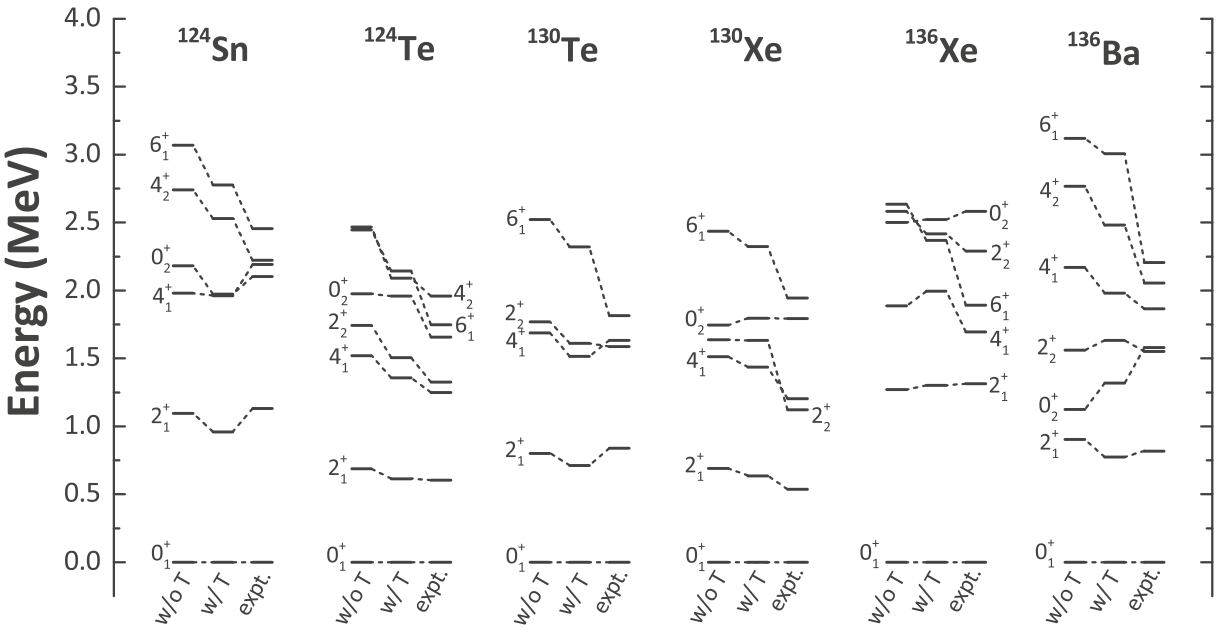

Fig. 1 Calculated low-lying energy levels for ^{124}Sn, ^{124}Te, ^{130}Te, ^{130}Xe, ^{136}Xe, and ^{136}Ba by using the PGCM employed the *jj*55 Hamiltonian excluding or including the tensor term, compared to the experimental data [55]

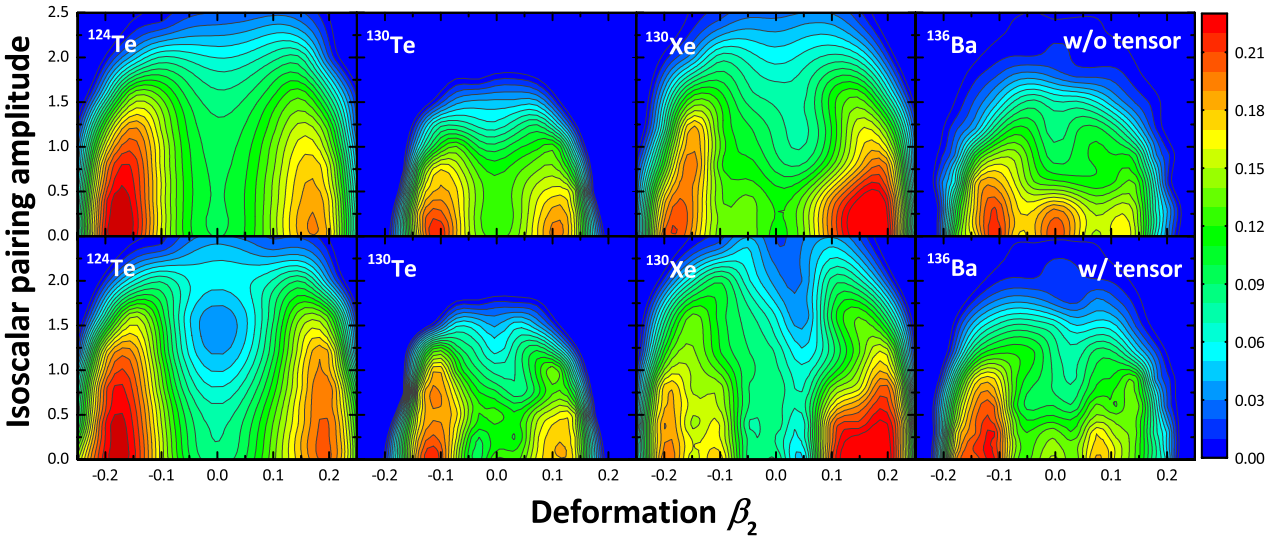

Fig. 3 (Color online) Square of the collective wave functions in ^{124}Te, ^{130}Te, ^{130}Xe, and ^{136}Ba calculated with the *jj*55 Hamiltonian excluding (upper panel) or including (lower panel) the tensor term

collective correlation and hence provides a better agreement with the experimentally adopted values of $B(E2)$. It should be noted that the increase in quadrupole collectivity is more significant in daughter nuclei, that is, ^{124}Te, ^{130}Xe, and ^{136}Ba. This leads to a larger deviation in the intrinsic deformation between the parent and daughter nuclei. The underlying physics will be discussed in more detail later in this paper.

We then computed the values of $0\nu\beta\beta$ decay matrix elements of ^{124}Sn, ^{130}Te, and ^{136}Xe. In closure approximation, the $0\nu\beta\beta$ matrix element of a two-body transition operator is computed between the initial and final ground states. Assuming an exchange of a light Majorana neutrino with the usual left-handed currents, the matrix element is [18]

$$M^{0\nu} = M^{0\nu}_{\mathrm{GT}} - \frac{g_V^2}{g_A^2} M^{0\nu}_{\mathrm{F}} + M^{0\nu}_{\mathrm{T}}, \tag{9}$$

where GT, F, and T refer to the Gamow–Teller, Fermi, and tensor parts of the matrix elements, respectively. A detailed presentation of the forms of Gamow–Teller, Fermi, and tensor transition operators can be found in Refs. [13, 18]. Note that the tensor transition operator is unrelated to the tensor term of the effective Hamiltonian. The vector and axial coupling constants are taken to be $g_{\mathrm{V}} = 1$ and $g_{\mathrm{A}} = 1.254$, respectively. Wave functions were modified at short distances using a Jastrow short-range correlation (SRC) function with CD-Bonn parametrization [18, 38].

The results are listed in Table 1, where the Gamow–Teller, Fermi, and tensor contributions are shown. While the Fermi parts remain almost unchanged, the Gamow–Teller parts are drastically suppressed when the tensor force is considered. The total matrix elements given by the calculation, including the tensor force, are approximately 26 to 40% smaller than those of the calculation excluding the tensor force.

Table 1 The nuclear matrix elements obtained for ^{124}Sn, ^{130}Te, and ^{136}Xe, employing the *jj*55 Hamiltonian excluding or including the tensor term

		$M^{0\nu}_{\mathrm{GT}}$	$M^{0\nu}_{\mathrm{F}}$	$M^{0\nu}_{\mathrm{T}}$	$M^{0\nu}$
^{124}Sn	w/o tensor	3.56	−0.64	−0.061	3.91
	w/ tensor	2.65	−0.64	−0.020	3.04
^{130}Te	w/o tensor	4.29	−0.75	−0.064	4.70
	w/ tensor	3.33	−0.65	−0.015	3.73
^{136}Xe	w/o tensor	3.26	−0.44	−0.046	3.49
	w/ tensor	2.17	−0.50	−0.009	2.48

CD-Bonn SRC parametrization was used

The tensor part of the NME, although suppressed if the tensor force is included, is negligibly small. This is in accordance with other studies that used different nuclear structural methods [23, 33, 42]. Therefore, tensor contributions were neglected [17, 19, 37]. The small tensor contributions in the NME are mainly attributed to the fact that the tensor part is induced by high-order currents. Thus, the two-body matrix elements of the tensor $0\nu\beta\beta$ decay operator are much smaller than those of Gamow–Teller and Fermi matrices. Because the value is small and subtle, it is difficult to trace the origin of these numerical changes in tensor NME. The interference between the collective correlations and tensor contributions in the NME remains unclear. Further study of the tensor part of the NME is required in the future, but its negligible contribution may not affect the conclusions we present in this work.

The influence of collective correlations on $0\nu\beta\beta$ nuclear matrix elements can be evaluated by the collective wave functions of the parent and daughter nuclei. The so-called collective wave functions are defined to account for the probability density of finding the state with a given expectation values of collective operators in Eq. (3). The detailed expression for the collective wave functions is given in the Eq. (18–19) of Ref. [53]. Note that the sum of collective wave functions is normalized to 1. When the probability density of finding the state with the specific deformation and isoscalar pairing amplitude increases, probability density of finding the state elsewhere would be suppressed consequently. Figure 3 shows the square of the collective wave functions against quadrupole deformation β_2 and isoscalar pn pairing amplitude. Since the cases ^{124}Sn and ^{136}Xe lack valence protons and valence neutron holes, respectively, and hence cannot change pn pairing, the squares of the collective wave functions of these two nuclei are not displayed. It can be seen that the largest peaks of collective wave functions in these nuclei are pushed, to some different extent, to the region with larger quadrupole deformations and isoscalar pairing amplitude if the tensor force is incorporated. The most apparent case is ^{136}Ba, where a subpeak appears at the sphericity in the calculation excluding the tensor force, but vanishes when we take the tensor force into consideration. Another interesting case occurs in ^{124}Te. When the tensor force is included, the increase of the collective wave functions with large quadrupole deformation and larger isoscalar pairing forms a dip in the region with near spherical deformation and intermediate isoscalar pairing. Since ^{124}Sn and ^{136}Xe keep their characteristics of sphericity owing to the $Z = 50$ and $N = 82$ shell closure, respectively, the difference of deformations between all the parent and their daughter nuclei are enlarged. In addition, the collective wave functions obtained with inclusion of the tensor force spread more widely along with the isoscalar pairing, indicating stronger isoscalar pairing fluctuations. The effects of both quadrupole deformation and isoscalar pairing therefore strongly hinder the $0\nu\beta\beta$ matrix elements.

To unveil the underlying connection among tensor force, collectivity, and nuclear matrix elements for $0\nu\beta\beta$ decay, the HFB effective single-particle energies (ESPEs) for valence neutron and proton orbits in ^{130}Te and ^{130}Xe are exhibited in Fig. 4. In this work, the HFB single-particle energies are obtained by diagonalizing the HF Hamiltonian h in the HFB equation, which is constructed with the density matrix of the HFB solution. For simplicity, only the ESPEs at spherical shapes and with isoscalar pairing amplitude $\phi = 0$ are shown. Note that the ESPEs are plotted relative to the $2s_{1/2}$ orbits. The ESPE is changed by the tensor force itself, as well as by re-adjusting the one-body part of the effective interaction due to the exclusion of tensor force. By looking at relative ESPEs, one can partly remove the common

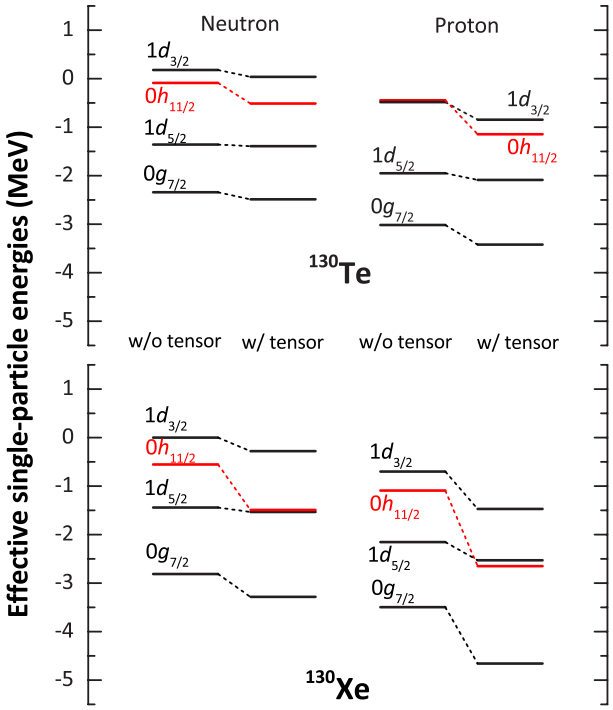

Fig. 4 (Color online) Neutron and proton effective single-particle energies in ^{130}Te and ^{130}Xe at spherical shape relative to $2s_{1/2}$ orbit, with exclusion and inclusion of tensor force

change from re-adjusting the one-body part of the effective interaction and thus can check the tensor effect more directly.

Figure 4 shows that owing to the inclusion of the tensor force, all neutron (proton) valence orbits are lowered with respect to the neutron (proton) $2s_{1/2}$ orbit. Among them, the neutron and proton $0h_{11/2}$ orbits were shifted more significantly. Of particular interest, the neutron and proton $0h_{11/2}$ orbits were suppressed more drastically in ^{130}Xe than in ^{130}Te. It is a complex many-body effect resulting from monopole interactions produced by the tensor force among all valence nucleon orbits. According to the rules discussed in Refs. [46, 66], the monopole interaction produced by the tensor force between proton $0g_{7/2}$ and neutron $0h_{11/2}$ orbit is attractive. As two more protons in ^{130}Xe mainly occupy the proton $0g_{7/2}$ orbit, the neutron $0h_{11/2}$ orbit decreases more remarkably than that in ^{130}Te. Meanwhile, the monopole interactions between the proton $0h_{11/2}$ and neutron $0h_{11/2}$, and between the proton $0h_{11/2}$ and neutron $1d_{5/2}$ orbits are both repulsive. Because the two neutrons are mainly removed from the neutron $0h_{11/2}$ and $1d_{5/2}$ orbits in ^{130}Xe when compared to ^{130}Te, the repulsive effects are weakened, and thus, the proton $0h_{11/2}$ orbit is pulled down more substantially. Similar results were observed for the ^{124}Sn/Te and ^{136}Xe/Ba.

For all investigated nuclei, the suppression of the proton $0h_{11/2}$ orbit lifts the proton Fermi surface, whereas the

lowering of the neutron $0h_{11/2}$ orbit pulls the neutron Fermi surface down. The Fermi surfaces of both protons and neutrons lie closer to the $0h_{11/2}$ midshell if the tensor force is included. It should be noted that high-j orbits are expected to exhibit a large deformation-driving effect [67, 68]. Because the lowering of $0h_{11/2}$ orbit is more significant in the daughter nuclei of $0\nu\beta\beta$ decays, the deformation-driving effect is larger, resulting in a more remarkable enhancement of the quadrupole correlations in these nuclei.

In addition, the shift of the valence nucleon orbits induced by the tensor force would adequately affect the nucleon occupancies. The change in the ground-state nucleon occupancies in the $0\nu\beta\beta$ decays provides an unquestionably important constraint on the calculation of the $0\nu\beta\beta$ matrix element, as it directly determines which neutrons decay, which protons are created in the decay, and how their configurations are re-arranged [69].

Recently, the proton occupancies and neutron vacancies of ^{130}Te and ^{130}Xe have been probed in single-nucleon transfer reactions to a level of precision corresponding to a few tenths of that of a nucleon [70, 71]. The total neutron vacancies measured are 4.16 for ^{130}Te and 6.26 for ^{130}Xe [70]; the total proton occupancies are 1.89 for ^{130}Te and 3.95 for ^{130}Xe [71], which gives the total change in proton occupancies and neutron vacancies of 2.06 and 2.10, respectively. Note that, in a realistic nucleus, nucleons may occupy orbits above the valence space or unoccupied orbits frozen in the core. Therefore, the measured total proton occupancy and neutron vacancy slightly deviate from the expected values with respect to the valence space. Figure 5 shows our calculations describing the change in proton occupancies and neutron vacancies in the $0\nu\beta\beta$ decay of ^{130}Te→^{130}Xe system, compared to experimental data [70, 71] and two shell-model calculations using the GCN5082 interaction [23] and the SVD interaction [27]. Notwithstanding the notable discrepancies from the experimental values, our calculation qualitatively reproduces the two most important contributions of the valence orbits for the nucleons that switch from neutrons to protons. The largest change in proton occupancies occurs in the $0g_{7/2}$ orbit, and the second largest change occurs in the $1d$ orbit. Meanwhile, the largest change in neutron vacancies appears in the $1d$ orbit, and the second largest change is in the $0h_{11/2}$ orbit. Note that the inclusion of the tensor force improves the description of the change in occupation of nucleons. As shown in Fig. 5, our calculation that excludes the tensor force overestimates the change in the neutron vacancy of the $0h_{11/2}$ orbit. Taking into account the tensor force, the neutron $0h_{11/2}$ orbit is pulled down substantially and merges into the $1d_{5/2}$ subshell. It reduces the change of neutron vacancies in the $0h_{11/2}$ orbit but enhances the change in the $1d_{5/2}$ orbit, which is in accord with the measurement.

In Table 2, the calculated NMEs for the $0\nu\beta\beta$ decay of ^{124}Sn →^{124} Te , ^{130}Te →^{130} Xe , and ^{136}Xe →^{136} Ba

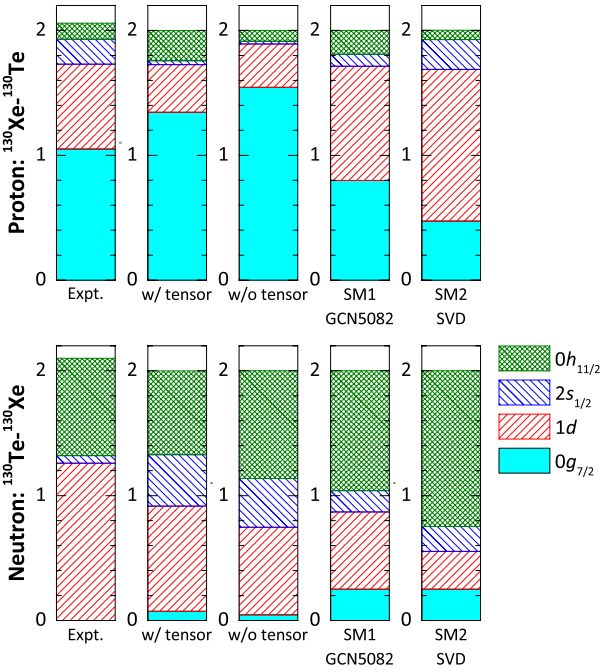

Fig. 5 (Color online) Change in proton occupancies and neutron vacancies between the ground states for the $0\nu\beta\beta$ decay of ^{130}Te→^{130}Xe. The experimental data [70, 71] are denoted "Expt.", compared to four different calculations: current works including and excluding the tensor force (denoted "w/ tensor" and "w/o tensor" respectively), shell-model calculations using GCN5082 interaction (denoted "SM1") [23] and SVD interaction (denoted "SM2") [27]

are compared with those given by ISM [23, 27, 28], QRPA [19, 40, 42], IBM2 [33], GCM in conjunction with the non-relativistic energy density functional (NR-EDF) [17], and relativistic energy density functional (R-EDF) [10]. In general, our $M^{0\nu}$'s are comparable with those obtained with the ISM, the QRPA from the Tübingen and Jyväskylä groups, and the IBM2, while the NR-EDF and R-EDF provide much larger values. The significantly large NMEs can be attributed to the lack of *pn* pairing correlation in the density energy functionals, either non-relativistic Gongny D1S [17] or relativistic PC-PK1 [10]. As previously mentioned, the *pn* pairing fluctuation would remarkably suppress the NMEs of $0\nu\beta\beta$ decays. The QRPA from the Chapel Hill group exhibited a noticeably small NME of ^{130}Te →^{130} Xe decay. This is because their QRPA calculation was based on a single HFB minimum, which was spherical for ^{130}Te and prolate for ^{130}Xe. The sharp deformation difference between the parent and daughter nuclei suppressed the suppression of $0\nu\beta\beta$ NME. Our PGCM calculations adequately addressed the fluctuations in shape and *pn* pairing on the same footing. This would fix the above issues and provide a reasonable description of the $0\nu\beta\beta$ NMEs.

Table 2 The NMEs for ^{124}Sn, ^{130}Te, and ^{136}Xe given by different nuclear structure methods: the ISM from the Strasbourg–Madrid (St-Ma) [23] and the Michigan (Mi) [27, 28] groups, the QRPA from the Tübingen (Tu) [40], the Jyväskylä (Jy) [42], and the Chapel Hill (Ch) [19] groups, the IBM2 [33], the GCM based on non-relativistic energy density functional (NR-EDF) [17] and relativistic energy density functional (R-EDF) [10], and present work

Models	This work	ISM (St-Ma)	ISM (Mi)	QRPA (Tu)	QRPA (Jy)	QRPA (Ch)	IBM2	NR-EDF	R-EDF
g_A	1.254	1.25	1.254	1.254	1.26	1.25	1.269	1.25	1.254
^{124}Sn $\rightarrow^{124}$ Te	3.04	2.62	2.00/2.15	2.56/2.91	5.30		3.19	5.79	4.33
^{130}Te $\rightarrow^{130}$ Xe	3.73	2.65	1.79/1.93	3.89/4.37	4.00	1.37/1.38	3.70	6.41	4.98
^{136}Xe $\rightarrow^{136}$ Ba	2.48	2.19	1.63/1.76	2.18/2.46	2.91	1.55/1.68	3.05	4.77	4.32

Two NME values separated by the slash sign denote the results obtained with Argonne V18 and CD-Bonn SRC

Finally, it should be mentioned that we only discuss the NME of $0\nu\beta\beta$ decay from the ground state of the parent nucleus to that of the daughter nucleus in this work. Actually, the decay to the low-lying excited states of the daughter nucleus should also be considered if it is allowed energetically. The NME of this process is strongly quenched by the phase-space factor in the standard light left-handed Majorana neutrino exchange mechanism [72, 73]. However, a considerable contribution to the NME from this process in the non-standard mechanism cannot be ruled out. Further study of $0\nu\beta\beta$ decay of NME to the lowest 2_1^+ state of the daughter nucleus within the framework of PGCM would be a desirable next step in the future.

5 Summary

An analysis of the influence of the monopole effect originating from the tensor force on both the collectivity and the nuclear matrix element of the $0\nu\beta\beta$ decay is presented for candidate isotopes ^{124}Sn/Te,^{130}Te/Xe, and ^{136}Xe/Ba, using the generator-coordinate method with a shell-model effective interaction. We employ an effective Hamiltonian written in terms of the monopole-based universal interaction V_{MU} plus a spin–orbit force taken from the M3Y interaction. The so-called monopole-based universal interaction consists of central and tensor forces explicitly, and hence, could clarify the effect of the tensor force by including or excluding the tensor-force term. The monopole effect arising from the tensor force is shown to have a significant influence on the quadrupole collectivity, nucleon occupancy, and $0\nu\beta\beta$ matrix element, which could be interpreted by the change in the shell structure owing to the novel feature of the tensor force. A better understanding and possible refinement of the tensor force would thus be of particular importance in reducing the theoretical uncertainty in the calculation of $0\nu\beta\beta$ nuclear matrix elements.

Author Contributions All authors contributed to the study conception and design. Material preparation, data collection, and analysis were performed by Chang-Feng Jiao and Cen-Xi Yuan. The first draft of the manuscript was written by Chang-Feng Jiao, and all authors commented on previous versions of the manuscript. All authors read and approved the final manuscript.

Data Availability The data that support the findings of this study are openly available in Science Data Bank at https://cstr.cn/31253.11.sciencedb.j00186.00745 and https://doi.org/10.57760/sciencedb.j00186.00745.

Conflict of interest Cen-Xi Yuan is an editorial board member for Nuclear Science and Techniques and was not involved in the editorial review, or the decision to publish this article. All authors declare that there are no Conflict of interest.

References

1. F.T. Avignone, S.R. Elliott, J. Engel, Double beta decay, Majorana neutrinos, and neutrino mass. Rev. Mod. Phys. **80**, 481–516 (2008). https://doi.org/10.1103/RevModPhys.80.481
2. W. Chen, L. Ma, J.H. Chen et al., Gamma-, neutron-, and muon-induced environmental background simulations for ^{100}Mo-based bolometric double-beta decay experiment at Jinping Underground Laboratory. Nucl. Sci. Tech. **34**, 135 (2023). https://doi.org/10.1007/s41365-023-01299-9
3. X.G. Cao, Y.L. Chang, K. Chen et al., (NνDEx-100 collaboration), NνDEx-100 conceptual design report. Nucl. Sci. Tech. **35**, 3 (2024). https://doi.org/10.1007/s41365-023-01360-7
4. L. Ma, H.Z. Huang, Y.G. Ma, Sensitivity challenge of the next-generation bolometric double-beta decay experiment. Research **7**, 0569 (2024). https://doi.org/10.34133/research.0569
5. The CUORE Collaboration, Search for Majorana neutrinos exploiting millikelvin cryogenics with CUORE. Nature **604**, 53–58 (2022). https://doi.org/10.1038/s41586-022-04497-4
6. J. Menéndez, Neutrinoless $\beta\beta$ decay mediated by the exchange of light and heavy neutrinos: The role of nuclear structure correlations. J. Phys. G Nucl. Part. Phys. **45**, 014003 (2017). https://doi.org/10.1088/1361-6471/aa9bd4
7. J. Engel, J. Menéndez, Status and future of nuclear matrix elements for neutrinoless double-beta decay: a review. Rep. Prog. Phys. **80**, 046301 (2017). https://doi.org/10.1088/1361-6633/aa5bc5
8. P. Vogel, Nuclear structure and double beta decay. J. Phys. G: Nucl. Part. Phys. **39**, 124002 (2012). https://doi.org/10.1088/0954-3899/39/12/124002
9. D.L. Fang, A. Faessler, V. Rodin et al., Neutrinoless double-β decay of deformed nuclei within quasiparticle random-phase

approximation with a realistic interaction. Phys. Rev. C **83**, 034320 (2011). https://doi.org/10.1103/PhysRevC.83.034320
10. J.M. Yao, L.S. Song, K. Hagino et al., Systematic study of nuclear matrix elements in neutrinoless double-β decay with a beyond-mean-field covariant density functional theory. Phys. Rev. C **91**, 024316 (2015). https://doi.org/10.1103/PhysRevC.91.024316
11. T.R. Rodríguez, G. Martínez-Pinedo, Energy density functional study of nuclear matrix elements for neutrinoless $\beta\beta$ decay. Phys. Rev. Lett. **105**, 252503 (2010). https://doi.org/10.1103/PhysRevLett.105.252503
12. T.R. Rodríguez, G. Martínez-Pinedo, Neutrinoless $\beta\beta$ decay nuclear matrix elements in an isotopic chain. Phys. Lett. B **719**, 174 (2013). https://doi.org/10.1016/j.physletb.2012.12.063
13. C.F. Jiao, J. Engel, J.D. Holt, Neutrinoless double-β decay matrix elements in large shell-model spaces with the generator-coordinate method. Phys. Rev. C **96**, 054310 (2017). https://doi.org/10.1103/PhysRevC.96.054310
14. J.M. Yao, J. Engel, Octupole correlations in low-lying states of ^{150}Nd and ^{150}Sm and their impact on neutrinoless double-β decay. Phys. Rev. C **94**, 014306 (2016). https://doi.org/10.1103/PhysRevC.94.014306
15. P. Vogel, M.R. Zirnbauer, Suppression of the two-neutrino double-beta decay by nuclear-structure effects. Phys. Rev. Lett. **57**, 3148 (1986). https://doi.org/10.1103/PhysRevLett.57.3148
16. J. Engel, P. Vogel, M.R. Zirnbauer, Nuclear structure effects in double-beta decay. Phys. Rev. C **37**, 731–746 (1988). https://doi.org/10.1103/PhysRevC.37.731
17. N.L. Vaquero, T.R. Rodríguez, J.L. Egido, Shape and pairing fluctuation effects on neutrinoless double beta decay nuclear matrix elements. Phys. Rev. Lett. **111**, 142501 (2013). https://doi.org/10.1103/PhysRevLett.111.142501
18. F. Šimkovic, A. Faessler, V. Rodin et al., Anatomy of the $0\nu\beta\beta$ nuclear matrix elements. Phys. Rev. C **77**, 045503 (2008). https://doi.org/10.1103/PhysRevC.77.045503
19. M.T. Mustonen, J. Engel, Large-scale calculations of the double-β decay of ^{76}Ge, ^{130}Te, ^{136}Xe, and ^{150}Nd in the deformed self-consistent Skyrme quasiparticle random-phase approximation. Phys. Rev. C **87**, 064302 (2013). https://doi.org/10.1103/PhysRevC.87.064302
20. N. Hinohara, J. Engel, Proton-neutron pairing amplitude as a generator coordinate for double-β decay. Phys. Rev. C **90**, 031301(R) (2014). https://doi.org/10.1103/PhysRevC.90.031301
21. J. Menéndez, N. Hinohara, J. Engel et al., Testing the importance of collective correlations in neutrinoless $\beta\beta$ decay. Phys. Rev. C **93**, 014305 (2016). https://doi.org/10.1103/PhysRevC.93.014305
22. E. Caurier, J. Menéndez, F. Nowacki et al., Influence of pairing on the nuclear matrix elements of the neutrinoless $\beta\beta$ decays. Phys. Rev. Lett. **100**, 052503 (2008). https://doi.org/10.1103/PhysRevLett.100.052503
23. J. Menéndez, A. Poves, E. Caurier et al., Disassembling the nuclear matrix elements of the neutrinoless $\beta\beta$ decay. Nucl. Phys. A **818**, 139 (2009). https://doi.org/10.1016/j.nuclphysa.2008.12.005
24. M. Horoi, S. Stoica, Shell model analysis of the neutrinoless double-β decay of ^{48}Ca. Phys. Rev. C **81**, 024321 (2010). https://doi.org/10.1103/PhysRevC.81.024321
25. M. Horoi, Shell model analysis of competing contributions to the double-β decay of ^{48}Ca. Phys. Rev. C **87**, 014320 (2013). https://doi.org/10.1103/PhysRevC.87.014320
26. M. Horoi, B.A. Brown, Shell-model analysis of the ^{136}Xe double beta decay nuclear matrix elements. Phys. Rev. Lett. **110**, 222502 (2013). https://doi.org/10.1103/PhysRevLett.110.222502
27. A. Neacsu, M. Horoi, Shell model studies of the ^{130}Te neutrinoless double-β decay. Phys. Rev. C **91**, 024309 (2015). https://doi.org/10.1103/PhysRevC.91.024309
28. M. Horoi, A. Neacsu, Shell model predictions for ^{124}Sn double-β decay. Phys. Rev. C **93**, 024308 (2016). https://doi.org/10.1103/PhysRevC.93.024308
29. Y. Iwata, N. Shimizu, T. Otsuka et al., Large-scale shell-model analysis of the neutrinoless $\beta\beta$ decay of ^{48}Ca. Phys. Rev. Lett. **116**, 112502 (2016). https://doi.org/10.1103/PhysRevLett.116.112502
30. R.A. Sen'kov, M. Horoi, Shell-model calculation of neutrinoless double-β decay of ^{76}Ge. Phys. Rev. C **93**, 044334 (2016). https://doi.org/10.1103/PhysRevC.93.044334
31. J. Barea, J. Kotila, F. Iachello, Limits on neutrino masses from Neutrinoless double-β decay. Phys. Rev. Lett. **109**, 042501 (2012). https://doi.org/10.1103/PhysRevLett.109.042501
32. J. Barea, J. Kotila, F. Iachello, Nuclear matrix elements for double-β decay. Phys. Rev. C **87**, 014315 (2013). https://doi.org/10.1103/PhysRevC.87.014315
33. J. Barea, J. Kotila, F. Iachello, $0\nu\beta\beta$ and $2\nu\beta\beta$ nuclear matrix elements in the interacting boson model with isospin restoration. Phys. Rev. C **91**, 034304 (2015). https://doi.org/10.1103/PhysRevC.91.034304
34. F. Šimkovic, G. Pantis, J.D. Vergados et al., Additional nucleon current contributions to neutrinoless double β decay. Phys. Rev. C **60**, 055502 (1999). https://doi.org/10.1103/PhysRevC.60.055502
35. V.A. Rodin, A. Faessler, F. Šimkovic et al., Uncertainty in the $0\nu\beta\beta$ decay nuclear matrix elements. Phys. Rev. C **68**, 044302 (2003). https://doi.org/10.1103/PhysRevC.68.044302
36. M. Kortelainen, O. Civitarese, J. Suhonen et al., Short-range correlations and neutrinoless double beta decay. Phys. Lett. B **647**, 128 (2007). https://doi.org/10.1016/j.physletb.2007.01.054
37. M. Kortelainen, J. Suhonen, Improved short-range correlations and $0\nu\beta\beta$ nuclear matrix elements of ^{76}Ge and ^{82}Se. Phys. Rev. C **75**, 051303(R) (2007). https://doi.org/10.1103/PhysRevC.75.051303
38. F. Šimkovic, A. Faessler, H. Müther et al., $0\nu\beta\beta$-decay nuclear matrix elements with self-consistent short-range correlation. Phys. Rev. C **79**, 055501 (2009). https://doi.org/10.1103/PhysRevC.79.055501
39. F. Šimkovic, A. Faessler, P. Vogel, $0\nu\beta\beta$ nuclear matrix elements and the occupancy of individual orbits. Phys. Rev. C **79**, 015502 (2009). https://doi.org/10.1103/PhysRevC.79.015502
40. F. Šimkovic, V. Rodin, A. Faessler et al., $0\nu\beta\beta$ and $2\nu\beta\beta$ nuclear matrix elements, quasiparticle random-phase approximation, and isospin symmetry restoration. Phys. Rev. C **87**, 045501 (2013). https://doi.org/10.1103/PhysRevC.87.045501
41. A. Faessler, M. González, S. Kovalenko et al., Arbitrary mass Majorana neutrinos in neutrinoless double beta decay. Phys. Rev. D **90**, 096010 (2014). https://doi.org/10.1103/PhysRevD.90.096010
42. J. Hyvärinen, J. Suhonen, Nuclear matrix elements for $0\nu\beta\beta$ decays with light or heavy Majorana-neutrino exchange. Phys. Rev. C **91**, 024613 (2015). https://doi.org/10.1103/PhysRevC.91.024613
43. D.-L. Fang, A. Faessler, F. Šimkovic, $0\nu\beta\beta$-decay nuclear matrix element for light and heavy neutrino mass mechanisms from deformed quasiparticle random-phase approximation calculations for ^{76}Ge,^{82} Se,^{130} Te,^{136} Xe, and ^{150}Nd with isospin restoration. Phys. Rev. C **97**, 045503 (2018). https://doi.org/10.1103/PhysRevC.97.044503
44. C.F. Jiao, M. Horoi, A. Neacsu, Neutrinoless double-β decay of ^{124}Sn, ^{130}Te, and ^{136}Xe in the Hamiltonian-based generator-coordinate method. Phys. Rev. C **98**, 064324 (2018). https://doi.org/10.1103/PhysRevC.98.064324
45. C.F. Jiao, C.W. Johnson, Union of rotational and vibrational modes in generator-coordinate-type calculations, with application to neutrinoless double-β decay. Phys. Rev. C **100**, 031303(R) (2019). https://doi.org/10.1103/PhysRevC.100.031303

46. T. Otsuka, T. Suzuki, R. Fujimoto et al., Evolution of nuclear shells due to the tensor force. Phys. Rev. Lett. **95**, 232502 (2005). https://doi.org/10.1103/PhysRevLett.95.232502
47. T. Otsuka, T. Suzuki, M. Honma et al., Novel features of nuclear forces and shell evolution in exotic nuclei. Phys. Rev. Lett. **104**, 012501 (2010). https://doi.org/10.1103/PhysRevLett.104.012501
48. F. Minato, C.L. Bai, Impact of tensor force on β decay of magic and semimagic nuclei. Phys. Rev. Lett. **110**, 122501 (2013). https://doi.org/10.1103/PhysRevLett.110.122501
49. L. Si, Z.K. Cheng, A. Abdukerim et al., Determination of double beta decay half-life of ^{136}Xe with the PandaX-4T natural xenon detector. Research **2022**, 9798721 (2022). https://doi.org/10.34133/2022/9798721
50. A. Abdukerim et al., PandaX-xT-A deep underground multi-tentonne liquid xenon observatory. Sci. China Phys. Mech. Astron. **68**, 221011 (2025). https://doi.org/10.1007/s11433-024-2539-y
51. G. Bertsch, J. Borysowicz, H. McManus et al., Interactions for inelastic scattering derived from realistic potentials. Nucl. Phys. A **284**, 399 (1977). https://doi.org/10.1016/0375-9474(77)90392-X
52. P. Ring, P. Schuck, *The Nuclear Many-Body Problem* (Springer-Verlag, Berlin, 1980)
53. T.R. Rodríguez, J.L. Egido, Triaxial angular momentum projection and configuration mixing calculations with the Gogny force. Phys. Rev. C **81**, 064323 (2010). https://doi.org/10.1103/PhysRevC.81.064323
54. J.M. Yao, J. Meng, P. Ring et al., Configuration mixing of angular-momentum-projected triaxial relativistic mean-field wave functions. Phys. Rev. C **81**, 044311 (2010). https://doi.org/10.1103/PhysRevC.81.044311
55. "Nudat 3.0," https://www.nndc.bnl.gov/nudat3/
56. C. Yuan, T. Suzuki, T. Otsuka et al., Shell-model study of boron, carbon, nitrogen, and oxygen isotopes with a monopole-based universal interaction. Phys. Rev. C **85**, 064324 (2012). https://doi.org/10.1103/PhysRevC.85.064324
57. Y. Utsuno, T. Otsuka, B.A. Brown et al., Shape transitions in exotic Si and S isotopes and tensor-force-driven Jahn-Teller effect. Phys. Rev. C **86**, 051301(R) (2012). https://doi.org/10.1103/PhysRevC.86.051301
58. T. Togashi, N. Shimizu, Y. Utsuno et al., Large-scale shell-model calculations for unnatural-parity high-spin states in neutron-rich Cr and Fe isotopes. Phys. Rev. C **91**, 024320 (2015). https://doi.org/10.1103/PhysRevC.91.024320
59. C.X. Yuan, Z. Liu, F.R. Xu et al., Isomerism in the "south-east'' of ^{132}Sn and a predicted neutron-decaying isomer in ^{129}Pd. Phys. Lett. B **762**, 237 (2016). https://doi.org/10.1016/j.physletb.2016.09.030
60. C.X. Yuan, M.L. Liu, N. Shimizu et al., Shell-model study on spectroscopic properties in the region "south'' of ^{208}Pb. Phys. Rev. C **106**, 044314 (2022). https://doi.org/10.1103/PhysRevC.106.044314
61. Z.Y. Zhang, H.B. Yang, M.H. Huang et al., New α-emitting isotope ^{214}U and abnormal enhancement of alpha-particle clustering in lightest uranium isotopes. Phys. Rev. Lett. **126**, 152502 (2021). https://doi.org/10.1103/PhysRevLett.126.152502
62. H.B. Yang, Z.G. Gan, Z.Y. Zhang et al., New isotope ^{207}Th and odd-even staggering in α-decay energies for nuclei with $Z > 82$ and $N < 126$. Phys. Rev. C **105**, L051302 (2022). https://doi.org/10.1103/PhysRevC.105.L051302
63. C.X. Yuan, Y.L. Ge, M.L. Liu et al., Shell-model explanation on some newly discovered isomers. EPJ Web Conf. **239**, 04002 (2020). https://doi.org/10.11804/NuclPhysRev.37.2019CNPC18
64. M. Liu, C. Yuan, Recent progress in configuration-interaction shell model. Int. J. Mod. Phys. E **32**, 12 (2023). https://doi.org/10.1142/S0218301323300035
65. B. Pritychenko, M. Birch, B. Singh et al., Tables of $E2$ transition probabilities from the first 2^+ states in even-even nuclei. At. Data Nucl. Data Tables **107**, 1 (2016). https://doi.org/10.1016/j.adt.2015.10.001
66. T. Otsuka, T. Suzuki, M. Honma et al., Novel features of nuclear forces and shell evolution in exotic nuclei. Phys. Rev. Lett. **104**, 012501 (2010). https://doi.org/10.1103/PhysRevLett.104.012501
67. E.S. Paul, C.W. Beausang, D.B. Fossan et al., Collective oblate band in ^{131}La due to the rotational alignment of $h_{11/2}$ neutrons. Phys. Rev. Lett. **58**, 984 (1987). https://doi.org/10.1103/PhysRevLett.58.984
68. E.S. Paul, R. Ma, C.W. Buausang et al., Deformation-driving properties of the vi $_{\frac{13}{2}}[660]\frac{1}{2}^+$ intruder orbital for $A \simeq 130$ nuclei. Phys. Rev. Lett. **61**, 42 (1988). https://doi.org/10.1103/PhysRevLett.61.42
69. J.P. Schiffer, S.J. Freeman, J.A. Clark et al., Nuclear structure relevant to neutrinoless double β decay: ^{76}Ge and ^{76}Se. Phys. Rev. Lett. **100**, 112501 (2008). https://doi.org/10.1103/PhysRevLett.100.112501
70. B.P. Kay, T. Bloxham, S.A. McAllister et al., Valence neutron properties relevant to the neutrinoless double-β decay of ^{130}Te. Phys. Rev. C **87**, 011302(R) (2013). https://doi.org/10.1103/PhysRevC.87.011302
71. J.P. Entwisle, B.P. Kay, A. Tamii et al., Change of nuclear configurations in the neutrinoless double-β decay of ^{130} Te $\rightarrow^{130}$ Xe and ^{136} Xe $\rightarrow^{136}$ Ba. Phys. Rev. C **93**, 064312 (2016). https://doi.org/10.1103/PhysRevC.93.064312
72. T. Tomoda, $0^+ \rightarrow 2^+$ neutrinoless $\beta\beta$ decay of ^{76}Ge. Nucl. Phys. A **484**, 635 (1988). https://doi.org/10.1016/0375-9474(88)90313-2
73. D.-L. Fang, A. Faessler, Nuclear matrix elements for the $0\nu\beta\beta(0^+ \rightarrow 2^+)$ decay of ^{76}Ge within the two-nucleon mechanism. Phys. Rev. C **103**, 045501 (2021). https://doi.org/10.1103/PhysRevC.103.045501